Supporting information for:

Improving the aggregation of layer-by-layer processed all-polymer solar cells with additive during the film deposition and thermal annealing

Luzhuo Li[1,2], Hanyue Gao[1,2], Mingyu Zuo[1,2], Yu Shen[1,2], Qiang Zhang[1*] and Yanchun Han[1,2*]

[1]State Key Laboratory of Polymer Physics and Chemistry, Changchun Institute of Applied Chemistry, Chinese Academy of Sciences, Changchun 130022, China

[2]School of Applied Chemistry and Engineering, University of Science and Technology of China, Hefei, 230026, China

E-mail: zhqawh@ciac.ac.cn (Qiang Zhang)

ychan@ciac.ac.cn (Yanchun Han)

Supporting Information Contents

Experimental Part

Supplementary Figures

Figure S1. (a) TGA curves of the 2-MN, solid line represents the mass change of 2-MN under a heating rate of 2°C min^{-1}, dotted line represents the mass change of 2-MN under a heating rate of 2°C min^{-1} and held at 90 °C for 30 minutes. (b) FT-IR spectra of 2-MN, PM6, PY-IT, PM6/PY-IT, PM6/PY-IT (2-MN) before and after thermal annealing.

Figure S2. (a) Volatilization process of 2-MN on silicon dioxide substrate heated at 90 ℃. (b) Photos of polarizing microscope of 2-MN coated silicon dioxide substrate before and after thermal annealing at 90 ℃ for 5 minutes.

Figure S3. Cyclic voltammograms of PM6 and PY-IT measured in 0.1 $mol \cdot L^{-1}$ Bu_4NPF_6 acetonitrile solution.

Figure S4. UV-vis-NIR absorption spectra of active layer films with different contents of 2-MN.

Figure S5. Statistical evaluation of the device performance (10 devices) based on PM6/PY-IT with different contents of 2-MN.

Figure S6. (a) hole-only and (b) electron-only devices by SCLC method.

Figure S7. J_{sc} versus light intensity of the all-PSCs based on PM6/PY-IT, PM6/PY-IT (2-MN) and PM6:PY-IT (2-MN).

Figure S8. (a) AFM height images and (b) TEM images of PM6, PM6 (2-

MN), PY-IT and PY-IT (2-MN) films.

Figure S9. Film-depth-dependent light absorption spectra for PM6/PY-IT, PM6:PY-IT (2-MN) and PM6/PY-IT (2-MN) films.

Figure S10. Contact angle images of PM6, PY-IT and 2-MN films with (a) water and (b) diiodomethane droplet on top.

Figure S11. (a) In-situ 2D UV-vis-NIR absorption spectra and (b) the maximum absorption peak intensity over time of PM6, PM6 (2-MN), PY-IT and PY-IT (2-MN) films during film formation.

Figure S12. (a) In-situ UV-vis-NIR absorption spectra and (b) In-situ 2D UV-vis absorption spectra of PM6, PM6 (2-MN), PY-IT and PY-IT (2-MN) films during thermal annealing process.

Figure S13. In-situ UV-vis-NIR absorption spectra for the PM6/PY-IT, PM6:PY-IT (2-MN) and PM6/PY-IT (2-MN) during thermal annealing process.

Figure S14. Chemical structure of PM7, D18 and PY-DT.

Figure S15. Current-voltage (*J-V*) characteristics of (a) PM7/PY-IT, (b) PM7/PY-DT, (c) D18/PY-IT and (d) D18/PY-DT devices processed without and with 2-MN.

Figure S16. Statistical evaluation of the device performance (10 devices) based on (a) PM7/PY-IT, (b) PM7/PY-DT, (c) D18/PY-IT and (d) D18/PY-DT devices processed without and with 2-MN.

Supplementary Tables

Table S1. Photovoltaic parameters of the all-PSCs based on PM6/PY-IT with different contents of 2-MN.

Table S2. Detailed photovoltaic parameters of device based on PM6/PY-IT.

Table S3. Detailed photovoltaic parameters of device based on PM6/PY-IT (50 wt% 2-MN).

Table S4. Detailed photovoltaic parameters of device based on PM6/PY-IT (100 wt% 2-MN).

Table S5. Detailed photovoltaic parameters of device based on PM6/PY-IT (150 wt% 2-MN).

Table S6. Detailed photovoltaic parameters of device based on PM6/PY-IT (200 wt% 2-MN).

Table S7. Detailed photovoltaic parameters of device based on PM6:PY-IT (150 wt% 2-MN).

Table S8. Photovoltaic parameters of the all-PSCs based on PM6/PY-IT (2-MN) with thermal annealing at 80 ℃ for different annealing time.

Table S9. Photovoltaic parameters of the all-PSCs based on PM6/PY-IT (2-MN) with thermal annealing for 5 minutes at different temperatures.

Table S10. Exciton dissociation and charge collection parameters of the devices based on PM6/PY-IT, PM6:PY-IT, PM6/PY-IT (2-MN) and PM6:PY-IT (2-MN).

Table S11. The parameters of GIWAXS 1D profiles for the different films

of in-plane (100) diffraction peak.

Table S12. The parameters of GIWAXS 1D profiles for the different films of out-of-plane (010) diffraction peak.

Table S13. Contact angles and surface energies of PM6, PY-IT and 2-MN.

Table S14. Detailed photovoltaic performances of (a) PM7/PY-IT, (b) PM7/PY-DT, (c) D18/PY-IT and (d) D18/PY-DT devices processed without and with 2-MN.

Materials: Poly{[4,8-bis[5-(2-ethylhexyl)-4-fluoro-2-thienyl]benzo[1,2-b:4,5-b′]-dithiophene-2,6-diyl]-alt-[2,5-thiophenediyl[5,7-bis(2-ethylhexyl)-4,8-dioxo-4H,8H-benzo[1,2-c:4,5-c′]dithiophene-1,3-diyl]]} (PM6) was purchased from Orantec Ltd. The weight-average molecular (M_w), number-average molecular (M_n) and polydispersity index (PDI) were 42.6 kDa, 20.4 kDa and 2.27, respectively. (Poly[(2,2'((2Z,2'Z)-((12,13-bis(2-octyldodecyl)-3,9-diundecyl-12,13-dihydro[1,2,5]thiadiazolo[3,4e]thieno[200,300:40,50]thieno[20,30:4,5]pyrrolo[3,2-g]thieno[20,30:4,5]thieno[3,2-b]indole-2,10-diyl)bis(methanylylidene))bis(5-methyl-3-oxo-2,3-dihydro-1H-indene-2,1diylidene)) dimalononitrile-co-2,5-thiophene) (PY-IT) was purchased from Orantec Ltd. The M_w, M_n and PDI were 6.38 kDa, 3.36 kDa and 1.90, respectively. Acetone, isopropanol and chloroform were purchased from Xilong Scientific Co., LTD. Methanol was purchased from Sigma-Aldrich. 2-Methoxynaphthalene(2-MN) was purchased from TCI. They were all used as received.

Fabrication of all-PSCs: The devices were fabricated with conventional structure of ITO/PEDOT:PSS/active layer/PDINN/Ag. The ITO-coated glass substrate was successively precleaned with detergent, de-ionized water, acetone, isopropanol and de-ionized water. Ultrasound was performed for 20 minutes at one time. Subsequently, the ITO substrate surface is subjected to a drying process utilizing high-purity nitrogen gas.

The substrates were subjected to ultraviolet/ozone treatment for 25 minutes by UVO CLEANER model 144AX-220 Jelight Company Inc. For devices with PEDOT:PSS as the hole transporting layer (HTL), 20 nm PEDOT:PSS (Clevios P, VP Al 4083) was spin-coated at 5000 rpm onto the plasma-treated ITO substrates and baked at 140 °C for 15 minutes in air. The substrates were transferred to a nitrogen-filled glove box. For the fabrication of all-PSCs based on PM6/PY-IT device, the neat PM6 in chloroform (CF) (7 mg/mL) was spin-coated at 2000 rpm onto the PEDOT:PSS-coated substrates. And then PY-IT in chloroform (CF) (7 mg/mL) was subsequently spin-coated at 2500 rpm on top of the PM6 layer. For the PM6/PY-IT (2-MN) device, the neat PM6 in chloroform (CF) (7 mg/mL) with 10.5 mg/mL 2-MN was spin-coated at 2000 rpm onto the PEDOT:PSS-coated substrates. And then PY-IT in chloroform (CF) (7 mg/mL) with 10.5 mg/mL 2-MN was subsequently spin-coated at 2500 rpm on top of the PM6 layer. For the PM6:PY-IT (2-MN) device, the PM6:PY-IT (1:1) in chloroform (CF) (14 mg/mL) with 21 mg/mL 2-MN was spin-coated at 2000 rpm onto the PEDOT:PSS-coated substrates. The optimal thickness of PM6 and PY-IT were found to be 60 and 50 nm, respectively. The thicknesses of the entire active layers are about 105 nm for PM6/PY-IT and PM6/PY-IT (150 wt% 2-MN) devices. The thickness of the entire active layer is about 100 nm for PM6:PY-IT (150 wt% 2-MN) device. Thermal annealing was performed after the spin-coating of the

acceptor layer at 90 ℃ for 5 minutes. After that, a solution of PDINN in methanol with a concentration of 1.5 mg mL^{-1} was spin-coated onto the active layer in 3500 rpm for 30 s. Finally, Ag electrode of 150 nm thickness was evaporated in vacuum onto the cathode buffer layer at a pressure of 5×10^{-5} Pa. In our work, the typical active area of the devices was 5.4 mm^2.

Current density-voltage (*J-V*) characteristics: The *J-V* curves were measured on a computer-controlled Keithley 2400 source meter under 1 sun, AM1.5 G simulated solar illumination with a light intensity of 100 mW cm^{-2}. The testing bias was ranged from -0.5 to 1.2 V. The test was performed in a nitrogen-filled glovebox and the light intensity is calibrated with a standard silicon solar cell.

External quantum efficiency (EQE): The external quantum efficiency (EQE) spectra were obtained using the QE-R 3011 solar cell quantum efficiency testing system from Enli Tech. Co. in ambient condition. The testing range is 300-1000 nm. The instrument was stabilized for 25 minutes to stabilize the incident light. Then calibrated using a standard Si cell to perform EQE testing on the prepared OSC. This process was carried out in an air atmosphere.

Carrier mobility measurements: Carrier mobility and trap density were measured using the space-charge-limit current (SCLC) method. The electron mobility was determined with the device architecture of ITO/ZnO/active layer/PDINN/Ag and the hole mobility was determined

with the device architecture of ITO/PEDOT:PSS/ active layer/MoO_3/Ag. The mobility was determined by fitting the dark current to the model of a single carrier SCLC. The current density (J) - voltage (V) characteristics at space-charge-limited-current region can be described by the Mott-Gurney law:

$$J = \frac{9}{8}\varepsilon_r\varepsilon_0\varepsilon_0\frac{V^2}{d^3} \quad (1)$$

where J is the current, ε_0 is the permittivity of free space, ε_r is the relative permittivity of the material which is assumed to be 3 for organic semiconductors, μ_0 is the zero-field mobility, d is the thickness of the active layers, V is the effective voltage. The applied voltage is used without correcting for series resistance or built-in voltage. The carrier mobility can be calculated by fitting the dark current from the slope of the $J^{1/2} \sim V$ curves. The hole and electron mobilities are extracted with the fit parameters at an electric field (E) by the Murgatroyd equation:

$$\mu = \mu_0 e^{\gamma\sqrt{E}} \quad (2)$$

Contact angle measurement: The contact angle measurement was conducted to assess the wetting behavior of the organic films, providing insights into their surface properties. Under ambient conditions, contact angles of water and diiodomethane on various molecular films were determined using a contact angle goniometer (KRUSS GMBH, Germany DO3040). This analysis aimed to calculate the surface tension (γ) of each

molecule and the interaction parameters ($\chi_{a,b}$) between different molecules based on the Owens-Wendt theory.[49]

$$\gamma_s = \gamma_s^p + \gamma_s^d \quad (3)$$

$$(1 + \cos\theta_l)\gamma_l = 2\left(\sqrt{\gamma_l^d \gamma_s^d} + \sqrt{\gamma_l^p \gamma_s^p}\right) \quad (4)$$

In the equations, γ_s, γ_s^p, and γ_s^d are the total surface energy, polar component and dispersive component of surface energy, respecively; γ_l, γ_l^p and γ_l^d are the total surface energy, polar component and dispersive component of surface energy of the test liquid (water and diiodomethane), respectively. $\gamma_{diiodometh}$ = 50.8 mJ/m^2, γ_{water}= 72.8 mJ/m^2, γ_{water}^d = 21.8 mJ/m^2, γ_{water}^p = 51 mJ/m^2. The miscibility of two materials can be reflected by the Flory–Huggins interaction parameter (χ), which is obtained via using the equation:

$$\chi_{D,A} = \kappa\left(\sqrt{\gamma_D} - \sqrt{\gamma_A}\right)^2 \quad (5)$$

Cyclic voltammetry (CV): Cyclic voltammetry curves were carried out on a CHI660A electro-chemical work station. Using a standard three-electrode system, in this system, a glassy-carbon electrode, Ag/AgCl and platinum wire were used as a working electrode, counter electrode and reference electrode, respectively. The samples were spin coated on the working electrode to be tested. All electrodes were dipped in a 0.1 mol L^{-1} tetrabutylammonium hexafluorophosphate (Bu_4NPF_6) acetonitrile solution, with a scanning rate of 50 mV s^{-1}. Using ferrocene/ferrocenyl couple (Fc/Fc^+) to calibrate. The highest occupied molecular orbital (HOMO) and

lowest unoccupied molecular orbital (LUMO) energy levels can be calculated according to the oxidation potential (E_{ox}), reduction potential (E_{red}) and E_{Fc/Fc^+} with the equations:

$$E_{HOMO} = -\left(E_{ox} + 4.8 - E_{Fc/Fc^+}\right)eV \quad (6)$$

$$E_{LUMO} = -\left(E_{red} + 4.8 - E_{Fc/Fc^+}\right)eV \quad (7)$$

UV-vis absorption spectra: The ultraviolet-visible (UV-vis) absorption spectra were collected in the wavelength range of 400-1000 nm by a Lambda 750 spectrometer (Perkin-Elmer, Wellesley, MA). The film samples were spin-coated on ITO/PEDOT:PSS substrates under the same conditions as those used for device fabrication.

In-situ UV-vis Absorption spectra: In-situ UV-vis can be used to characterize the film formation aggreagation process from solution state to thin film state. The time interval between each spectral acquisition is 0.05 s, starting from the solution state and stopping after the film state stabilized.

Film-depth-dependent light absorption and composition distribution: For film-depth-dependent light-absorption spectra, the active layers were placed in an etching machine (Diener ZEPTO Plasma). It was found that a 7 nm thick thin film can be etched in about 90 s. After each etching, the light absorption characteristics of the active layer to different wavelengths of light were characterized by UV-vis absorption spectra. The process was repeated to obtain UV-visible absorption spectra at different etching depths.

Atomic force microscopy (AFM): The AFM measurement was performed with Bruker Dimension ICON AFM in peak force mode. The probe used for scanning was a silicon cantilever with an elastic constant of 2 N m^{-1} and a resonance frequency of ~ 70 kHz. The donor, acceptor and active layer films for the AFM characterization were prepared following the same procedure in the all-PSCs.

Transmission electron microscopy (TEM): The TEM images of active layers were obtained by a JEOL JEM-1400 transmission electron microscope operated at 120 kV. The active layers were spin coated onto the PEDOT:PSS-coated ITO substrates, then used the deionized water to dissolve the PEDOT:PSS layer and picked up the active layers using copper grids.

Grazing incidence wide-angle X-ray scattering (GIWAXS): The molecular arrangement and orientation behavior in the film were characterized using two-dimensional GIWAXS technique. GIWAXS data were obtained at beamline BL02U2 of Shanghai Synchrotron Radiation Facility (SSRF). The monochromatic of the light source was 1.24 Å. The incidence angle and exposure time are 0.3° and 10 s, respectively. The in-plane and out-of-plane 1D line profiles of were extracted from 2D scattering patterns using the GIWAXS-Tool software developed by beamline scientists. The position and FWHM of peaks were obtained by

fitting the peaks using Origin software. The samples were prepared on Si/PEDOT:PSS substrates

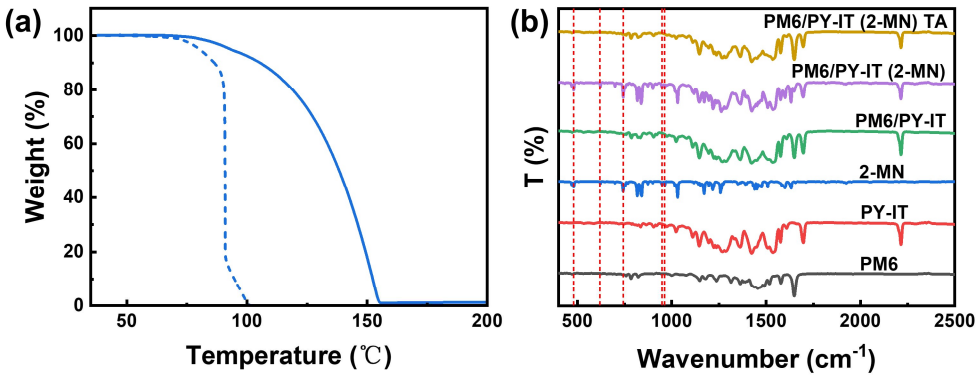

Figure S1. (a) TGA curves of the 2-MN, solid line represents the mass change of 2-MN under a heating rate of 2°C min^{-1}, dotted line represents the mass change of 2-MN under a heating rate of 2°C min^{-1} and held at 90°C for 30 minutes. (b) FT-IR spectra of 2-MN, PM6, PY-IT, PM6/PY-IT, PM6/PY-IT (2-MN) before and after thermal annealing.

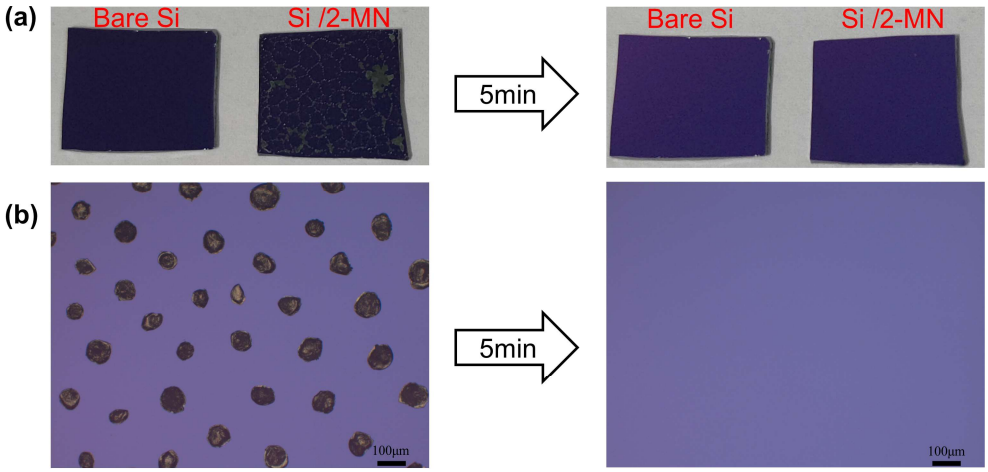

Figure S2. (a) Volatilization process of 2-MN on silicon dioxide substrate heated at 90 ℃. (b) Photos of polarizing microscope of 2-MN coated silicon dioxide substrate before and after thermal annealing at 90 ℃ for 5 min.

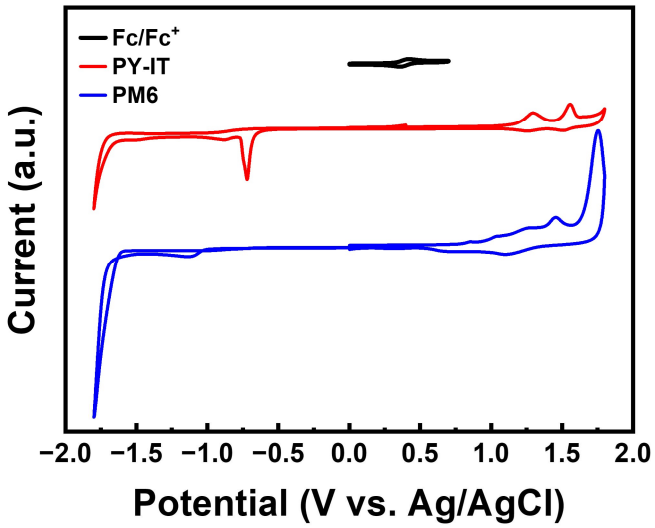

Figure S3. Cyclic voltammograms of PM6 and PY-IT measured in 0.1 mol·L^{-1} Bu_4NPF_6 acetonitrile solution.

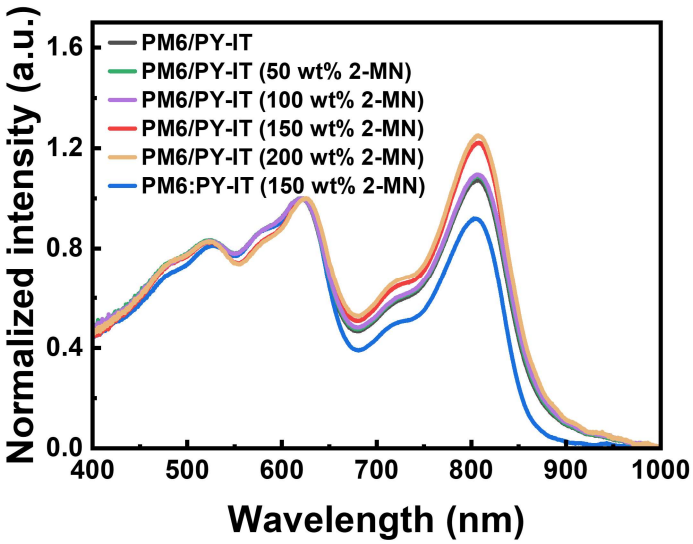

Figure S4. UV-vis-NIR absorption spectra of active layer films with different contents of 2-MN.

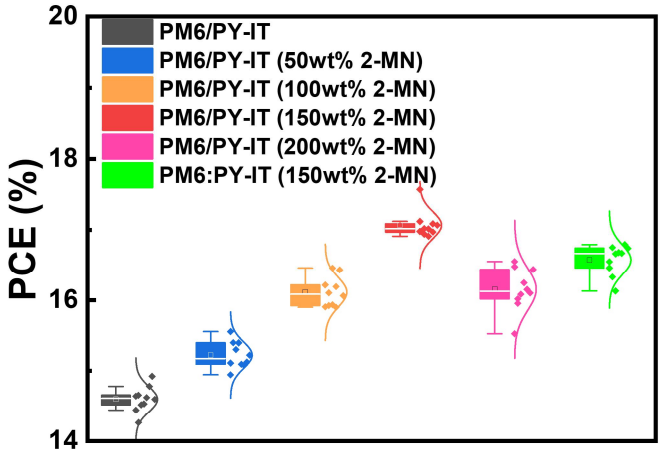

Figure S5. Statistical evaluation of the device performance (10 devices) based on PM6/PY-IT with different contents of 2-MN.

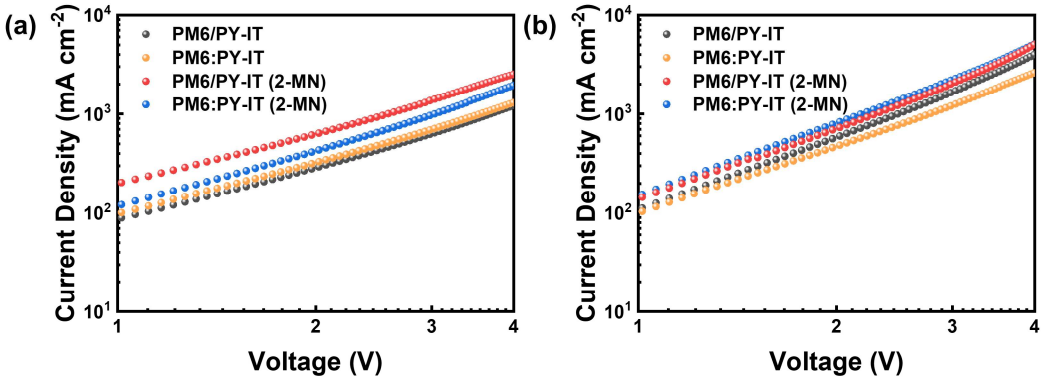

Figure S6. (a) hole-only and (b) electron-only devices by SCLC method.

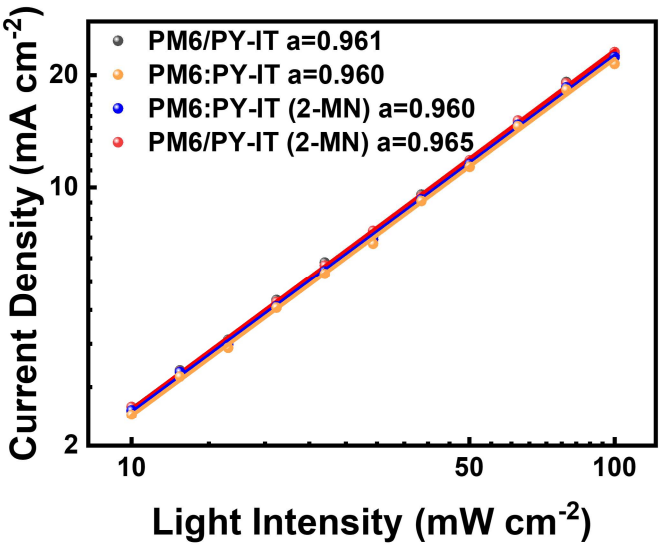

Figure S7. J_{sc} versus light intensity of the all-PSCs based on PM6/PY-IT, PM6:PY-IT, PM6/PY-IT (2-MN) and PM6:PY-IT (2-MN).

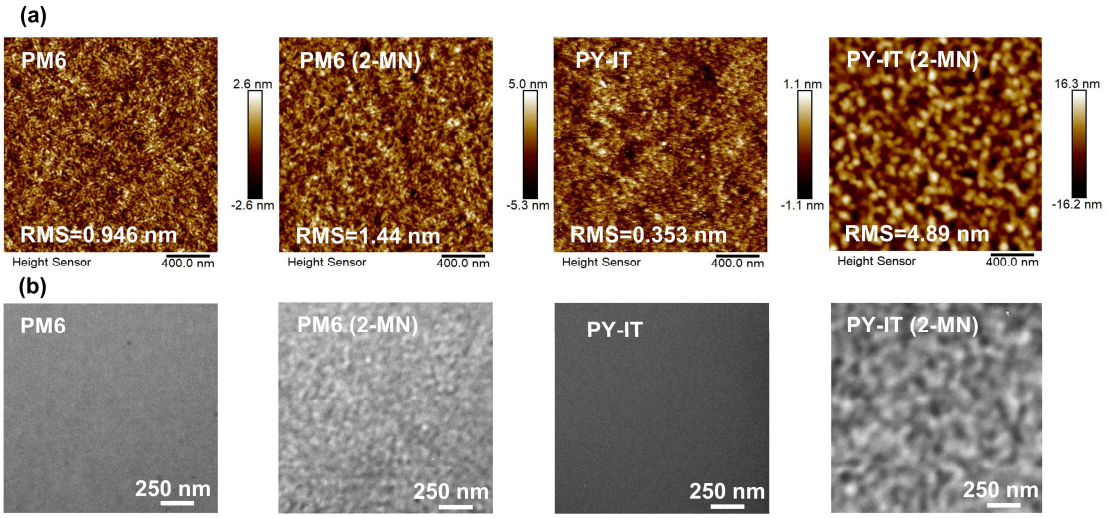

Figure S8. (a) AFM height images and (b) TEM images of PM6, PM6 (2-MN), PY-IT and PY-IT (2-MN) films.

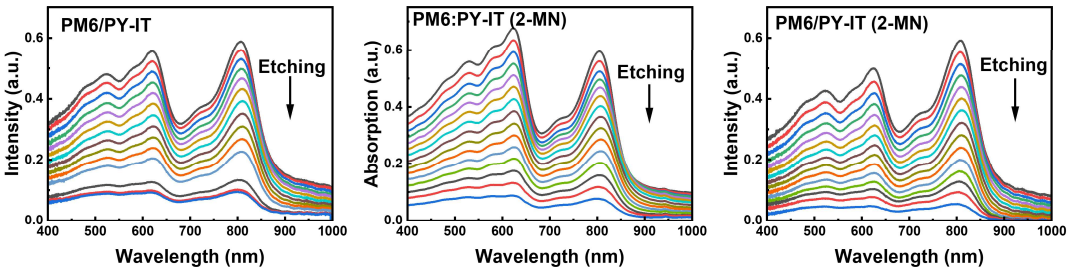

Figure S9. Film-depth-dependent light absorption spectra for PM6/PY-IT, PM6:PY-IT (2-MN) and PM6/PY-IT (2-MN) films.

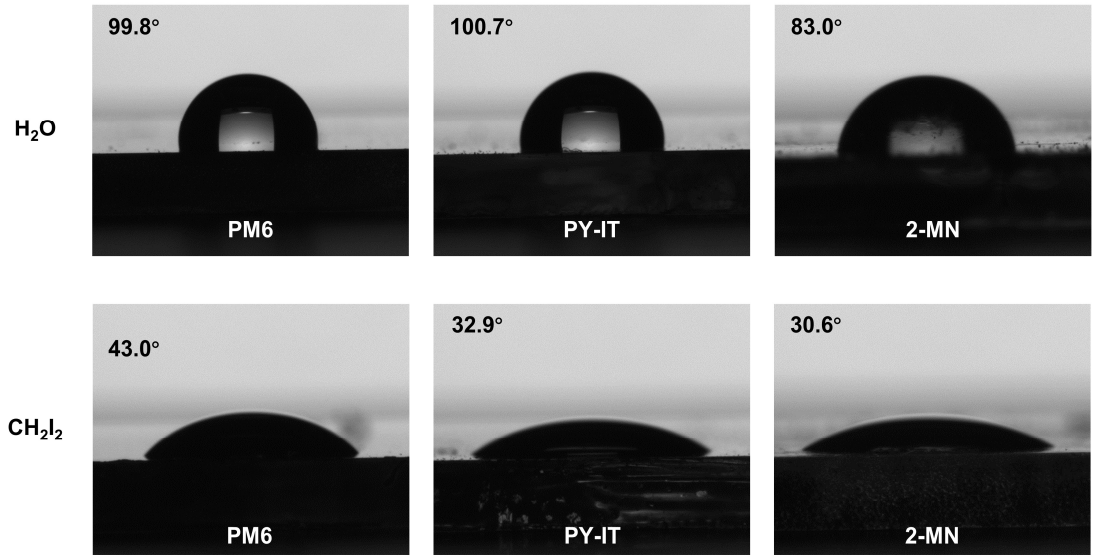

Figure S10. Contact angle images of PM6, PY-IT and 2-MN films with (a) water and (b) diiodomethane droplet on top.

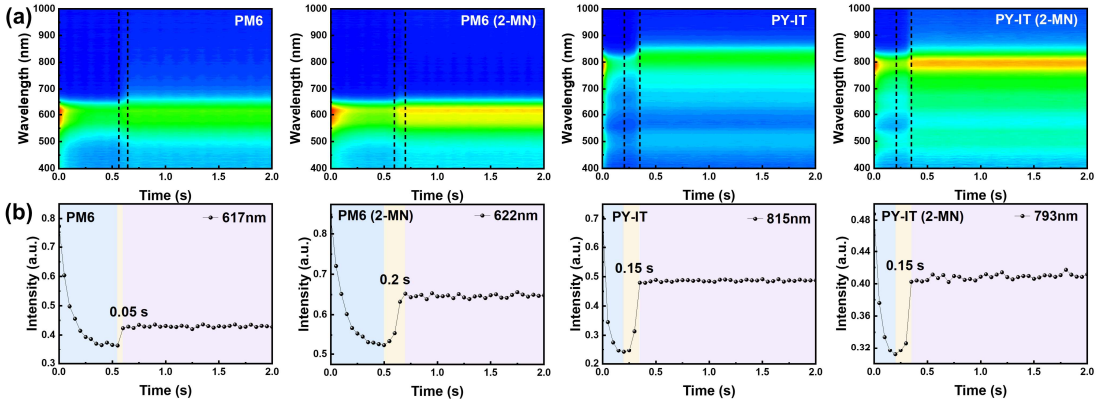

Figure S11. (a) In-situ 2D UV-vis-NIR absorption spectra and (b) the maximum absorption peak intensity over time of PM6, PM6 (2-MN), PY-IT and PY-IT (2-MN) films during film formation.

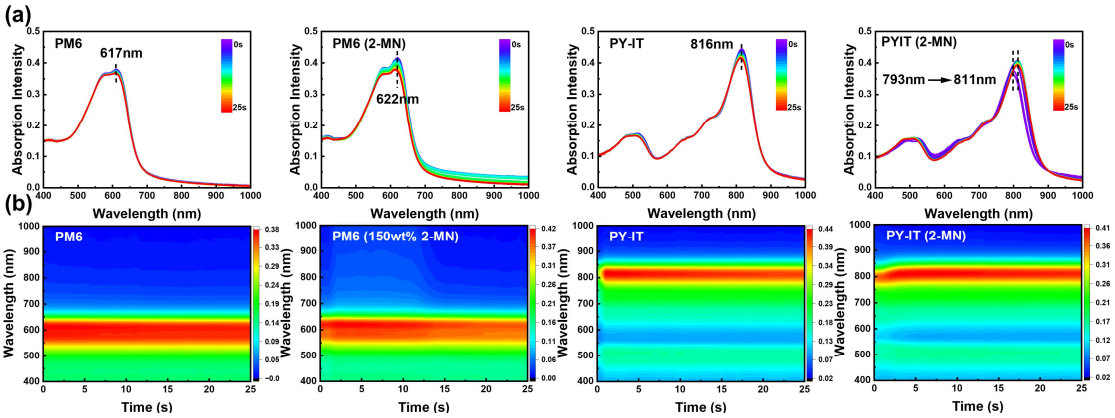

Figure S12. (a) In-situ UV-vis-NIR absorption spectra and (b) In-situ 2D UV-vis absorption spectra of PM6, PM6 (2-MN), PY-IT and PY-IT (2-MN) films during thermal annealing process.

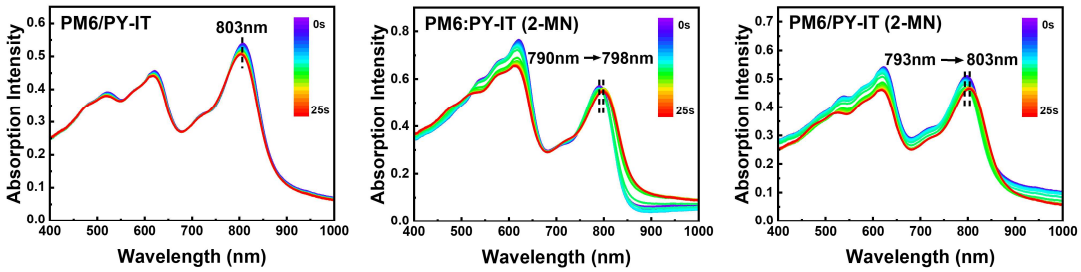

Figure S13. In-situ UV-vis-NIR absorption spectra for the PM6/PY-IT, PM6:PY-IT (2-MN) and PM6/PY-IT (2-MN) during thermal annealing process.

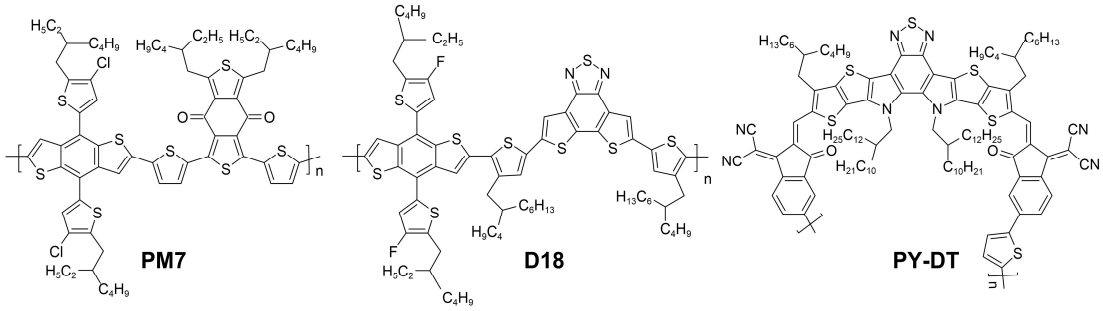

Figure S14. Chemical structure of PM7, D18 and PY-DT.

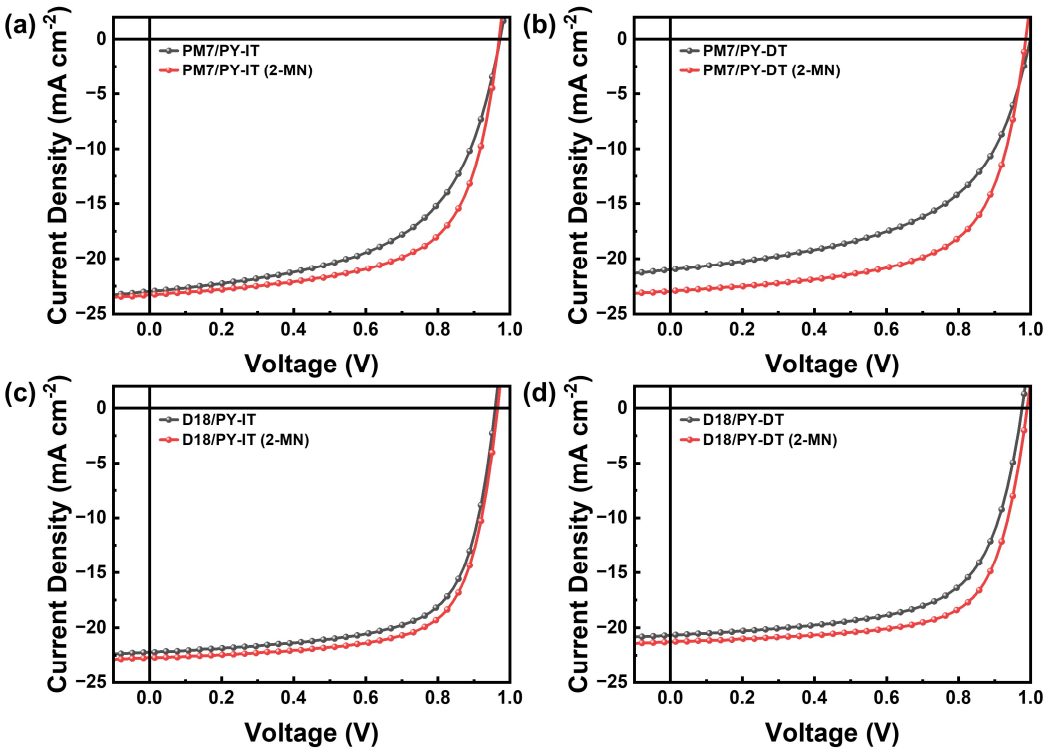

Figure S15. Current-voltage (*J-V*) characteristics of (a) PM7/PY-IT, (b) PM7/PY-DT, (c) D18/PY-IT and (d) D18/PY-DT devices processed without and with 2-MN.

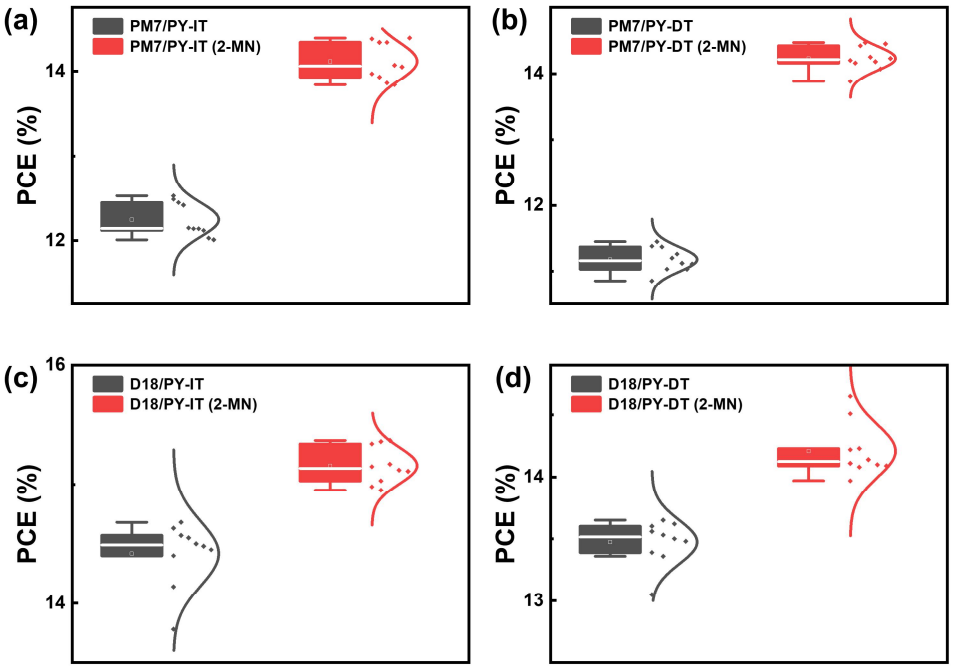

Figure S16. Statistical evaluation of the device performance (10 devices) based on (a) PM7/PY-IT, (b) PM7/PY-DT, (c) D18/PY-IT and (d) D18/PY-DT devices processed without and with 2-MN.

Table S1. Photovoltaic parameters of the all-PSCs based on PM6/PY-IT with different contents of 2-MN.

Conditions	V_{OC} (V)	J_{SC} (mA·cm^{-2})	FF (%)	PCE (%)
As cast	0.952 (0.947±0.003)	24.86 (24.58±0.18)	63.03 (62.71±0.44)	14.92 (14.60±0.19)
50wt% 2-MN	0.941 (0.939±0.005)	25.18 (24.88±0.33)	65.67 (65.16±0.93)	15.56 (15.22±0.19)
100wt% 2-MN	0.942 (0.938±0.004)	25.26 (24.95±0.24)	69.14 (68.84±0.32)	16.46 (16.11±0.21)
150wt% 2-MN	0.937 (0.939±0.003)	25.93 (25.06±0.44)	72.35 (72.56±1.03)	17.57 (17.07±0.20)
200wt% 2-MN	0.936 (0.931±0.002)	23.20 (22.09±0.44)	76.23 (75.17±0.86)	16.55 (16.16±0.30)

(a) The average values were obtained from at least ten devices.

Table S2. Detailed photovoltaic parameters of device based on PM6/PY-IT.

Number	V_{OC} (V)	J_{SC} (mA·cm^{-2})	FF (%)	PCE (%)
1	0.946	24.71	62.63	14.64
2	0.949	24.66	62.66	14.66
3	0.944	24.71	62.23	14.52
4	0.944	24.63	62.52	14.53
5	0.944	24.43	63.37	14.62
6	0.953	24.49	63.34	14.78
7	0.947	24.40	62.47	14.44
8	0.945	24.29	62.16	14.26
9	0.952	24.86	63.03	14.92
10	0.946	24.58	62.71	14.60

Table S3. Detailed photovoltaic parameters of device based on PM6/PY-IT (50 wt% 2-MN).

Number	V_{OC} (V)	J_{SC} (mA·cm^{-2})	FF (%)	PCE (%)
1	0.930	24.78	65.54	15.11
2	0.934	25.02	65.87	15.40
3	0.947	24.30	66.51	15.30
4	0.943	24.83	65.77	15.40
5	0.941	25.18	65.67	15.56
6	0.943	24.53	64.60	14.94
7	0.940	24.78	64.82	15.09
8	0.935	25.34	63.62	15.08
9	0.938	25.16	64.13	15.13
10	0.939	24.880	65.169	15.222

Table S4. Detailed photovoltaic parameters of device based on PM6/PY-IT (100 wt% 2-MN).

Number	V_{OC} (V)	J_{SC} (mA·cm^{-2})	FF (%)	PCE (%)
1	0.943	24.87	69.15	16.22
2	0.938	24.99	68.74	16.11
3	0.934	24.83	68.58	15.91
4	0.942	25.26	69.14	16.46
5	0.938	25.02	68.99	16.19
6	0.936	24.70	68.89	15.92
7	0.942	25.23	69.18	16.43
8	0.939	24.77	68.53	15.93
9	0.931	25.30	68.20	16.06
10	0.935	24.63	69.03	15.90

Table S5. Detailed photovoltaic parameters of device based on PM6/PY-IT (150 wt% 2-MN).

Number	V_{OC} (V)	J_{SC} (mA·cm^{-2})	FF (%)	PCE (%)
1	0.944	24.90	72.23	16.98
2	0.937	25.93	72.35	17.57
3	0.936	24.95	73.27	17.12
4	0.933	24.86	73.34	17.02
5	0.941	24.52	73.79	17.01
6	0.942	24.61	73.70	17.09
7	0.940	25.10	71.83	16.94
8	0.938	25.14	71.72	16.91
9	0.940	25.51	70.78	16.97
10	0.939	25.06	72.56	17.07

Table S6. Detailed photovoltaic parameters of device based on PM6/PY-IT (200 wt% 2-MN).

Number	V_{OC} (V)	J_{SC} (mA·cm^{-2})	FF (%)	PCE (%)
1	0.932	23.69	74.60	16.48
2	0.930	23.34	73.78	16.02
3	0.931	22.00	75.82	15.52
4	0.929	22.92	75.50	16.08
5	0.928	23.15	75.61	16.25
6	0.936	23.20	76.23	16.55
7	0.930	22.96	75.61	16.15
8	0.927	23.28	73.90	15.96
9	0.933	23.10	74.71	16.10
10	0.929	23.31	75.90	16.44

Table S7. Detailed photovoltaic parameters of device based on PM6:PY-IT (150 wt% 2-MN).

Number	V_{OC} (V)	J_{SC} (mA·cm^{-2})	FF (%)	PCE (%)
1	0.937	25.00	70.60	16.55
2	0.945	25.60	69.25	16.75
3	0.937	25.75	69.05	16.66
4	0.943	24.83	71.16	16.68
5	0.940	24.97	70.11	16.46
6	0.939	25.19	70.40	16.67
7	0.935	25.45	68.62	16.33
8	0.938	25.27	70.82	16.79
9	0.935	25.46	70.29	16.74
10	0.938	24.50	70.15	16.13

Table S8. Photovoltaic parameters of the all-PSCs based on PM6/PY-IT (2-MN) with thermal annealing at 80℃ for different annealing time.

TA duration (minutes)	V_{OC} (V)	J_{SC} (mA·cm^{-2})	FF (%)	PCE (%)
3	0.945	25.09	70.31	16.66
5	0.942	25.28	70.72	16.84
8	0.943	24.44	70.97	16.36
10	0.929	24.47	69.99	15.92

Table S9. Photovoltaic parameters of the all-PSCs based on PM6/PY-IT (2-MN) with thermal annealing for 5 minutes at different temperatures.

TA temperature (℃)	V_{OC} (V)	J_{SC} (mA·cm^{-2})	FF (%)	PCE (%)
80	0.942	25.28	70.72	16.84
90	0.939	25.51	70.78	16.97
100	0.927	25.33	70.06	16.46
110	0.930	25.15	69.88	16.36

Table S10. Exciton dissociation and charge collection parameters of the devices based on PM6/PY-IT, PM6:PY-IT, PM6/PY-IT (2-MN) and PM6:PY-IT (2-MN).

Conditions	J_{sat} (mA·cm^{-2})	J_{SC}* (mA·cm^{-2})	J_{max}& (mA·cm^{-2})	P_{diss} (%)	P_{coll} (%)
PM6/PY-IT	24.61	23.97	18.20	97.39	73.95
PM6:PY-IT	24.24	23.40	17.62	96.53	72.68
PM6/PY-IT (2-MN)	24.79	24.67	20.79	99.51	84.59
PM6:PY-IT (2-MN)	24.71	24.33	19.64	98.46	79.48

Table S11. The parameters of GIWAXS 1D profiles for the different films of in-plane (100) diffraction peak.

Conditions	(100)			
	q (Å^{-1})	d-spacing (Å)	FWHM (Å^{-1})	CCL (Å)
PM6	0.292	21.52	0.105	59.84
PM6 (2-MN)	0.290	21.67	0.058	108.33
PY-IT	0.357	17.60	0.156	40.30
PY-IT (2-MN)	0.347	18.11	0.176	35.70
PM6/PY-IT	0.337	18.64	0.140	44.88
PM6:PY-IT (2-MN)	0.295	21.30	0.094	66.80
PM6/PY-IT (2-MN)	0.292	21.52	0.064	98.17

Table S12. The parameters of GIWAXS 1D profiles for the different films of out-of-plane (010) diffraction peak.

Conditions	(010)			
	q (Å^{-1})	d-spacing (Å)	FWHM (Å^{-1})	CCL (Å)
PM6	-	-	-	-
PM6 (2-MN)	1.690	3.718	0.214	29.36
PY-IT	1.610	3.903	0.199	31.57
PY-IT (2-MN)	1.610	3.903	0.177	35.50
PM6/PY-IT	1.602	3.922	0.358	17.55
PM6:PY-IT (2-MN)	1.637	3.838	0.269	23.36
PM6/PY-IT (2-MN)	1.655	3.796	0.259	24.26

Table S13. Contact angles and surface energies of PM6, PY-IT and 2-MN.

Material	θ(°)		γ (mJ·m^{-2})			χ_{a-b}
	H_2O	CH_2I_2	γ_s^d	γ_s^p	γ_s	
PM6	99.8	43.0	38.07	0.04	38.11	0.35
PY-IT	100.7	32.9	42.98	0.02	43.00	0.04
2-MN	83.0	30.6	43.97	1.91	45.88	

Table S14. Detailed photovoltaic performances of (a) PM7/PY-IT, (b) PM7/PY-DT, (c) D18/PY-IT and (d) D18/PY-DT devices processed without and with 2-MN.

Conditions	V_{OC}/V	J_{SC}/mA•cm^{-2}	FF/%	PCE/%
PM7/PY-IT	0.972 (0.972±0.003)	22.98 (22.61±0.26)	56.05 (55.70±0.68)	12.53 (12.24±0.20)
PM7/PY-IT (2-MN)	0.963 (0.966±0.004)	23.58 (23.32±0.378)	63.27 (62.64±1.29)	14.38 (14.11±0.22)
PM7/PY-DT	1.000 (0.998±0.002)	20.79 (20.90±0.20)	54.50 (53.53±0.66)	11.38 (11.18±0.18)
PM7/PY-DT (2-MN)	0.986 (0.983±0.003)	22.98 (22.82±0.24)	63.82 (63.41±0.44)	14.47 (14.23±0.18)
D18/PY-IT	0.957 (0.958±0.005)	22.88 (22.49±0.55)	67.00 (66.92±2.33)	14.68 (14.41±0.26)
D18/PY-IT (2-MN)	0.965 (0.960±0.004)	23.73 (23.35±0.34)	67.56 (67.58±0.97)	15.36 (15.15±0.15)
D18/PY-DT	0.986 (0.984±0.005)	20.72 (20.59±0.21)	66.51 (66.44±0.87)	13.60 (13.47±0.17)
D18/PY-DT (2-MN)	0.989 (0.987±0.004)	21.27 (21.27±0.28)	69.56 (67.64±0.92)	14.65 (14.21±0.21)